Low-Voltage Driven MEMS VOA Using Torsional Attenuation Mechanism Based on Piezoelectric Beam Actuators

Kah How Koh, Takeshi Kobayashi, and Chengkuo Lee, *Member, IEEE*

***Abstract*—A gold-coated silicon mirror (5 mm $\times$ 5 mm) driven by a piezoelectric $Pb(Zr, Ti)O_3$ (PZT) beam with 1×10 cantilever actuators has been demonstrated for variable optical attenuator application. A dual-core-fiber collimator is aligned perpendicularly to the mirror in a three-dimensional light attenuation arrangement. Torsional attenuation based on the difference in the dc biasing voltage applied to the ten piezoelectric cantilevers was investigated. The attenuation curve under dc bias follows that of a Gaussian distribution, with dynamic attenuation range of 40 dB achieved at 1.8 V.**

***Index Terms*—Microelectromechanical Systems (MEMS), mirror, optical MEMS, piezoelectric Actuator, $Pb(Zr, Ti)O_3$ (PZT), variable optical attenuator (VOA).**

I. Introduction

MICROELECTROMECHANICAL systems (MEMS) technology has been an enabling tool for numerous telecommunication components in modern optical network systems based on dense-wavelength-division-multiplexed (DWDM) technology. The phenomenal growth of the internet in the past decade has led to telecommunication companies making huge investments in MEMS devices such as tunable lasers [1], optical switches [2], reconfigurable add–drop multiplexers [3], and variable optical attenuators (VOAs) [4], [5]. MEMS VOAs have been one of the most attractive devices in the optical communication market due to their widespread presence in optical networks. A large number of VOAs are currently used in the wavelength multiplexing (MUX) and demultiplexing (DMUX) nodes of DWDM system to control the transmission power of optical signals.

Most of the designs of VOAs reported in the literature adopted attenuation schemes that can be generally classified into three groups: shutter-type [5]–[7], planar reflective-type [8], [9], and three-dimensional (3-D) reflective-type [10]–[12]. Design of optics and their integration with large reflective mirrors are typically realized in 3-D configurations. In conjunction with large micro-optics such as dual-core collimators, the enabled 3-D VOA devices can gain excellent data of return loss, polarization-dependent loss (PDL), and wavelength-dependent loss (WDL) under reasonable driving voltage. To achieve large mechanical rotation angles, gimbaled mirrors using torsion bars or springs are the popular design for integration with various actuation mechanisms such as electrostatic [10], [11] and piezoelectric [12].

Limited research effort has been reported in 3-D MEMS VOAs in contrast to the reported activities in planar MEMS VOAs. Thus, in this work, we explore a new 3-D MEMS VOA driven by a piezoelectric beam actuator integrated with 1×10 $Pb(Zr, Ti)O_3$ (PZT) cantilever array. A novel torsional attenuation based on different dc biasing voltage applied to individual piezoelectric cantilever actuator on a cantilever beam is demonstrated. This actuation mechanism differs greatly from those actuation mechanisms of gimbaled mirror in torsional mode, i.e., the mirror rotation is generated against to the torsion spring or torsion bar. Although thermal bimorph beam actuator has been well-characterized in terms of their capability to generate large deflection, i.e., in bending mode [13], it was only until recently that a small torsional mirror driven by two separate thermal actuators has been reported [14]. A torsional mirror using beam actuator has not been reported so far. Instead of using a thermal bimorph beam actuator, our unique design of single beam actuator with integrated 1×10 piezoelectric cantilevers is the first successful demonstration of large torsion mirror actuation. In addition, the torsional motion of the mirror would not induce the displacement of the reflection point as most bending mirrors do. This makes VOA optical alignment straightforward and easy.

II. Device Description

A schematic diagram of the PZT 3-D MEMS VOA demonstrated in this letter is shown in Fig. 1(a). The device is micromachined from a silicon-on-insulator (SOI) substrate of 5-μm-thick Si device layer, with multilayers of Ti–Pt–$LaNiO_3$–PZT–$LaNiO_3$–Ti–Pt deposited as electrode materials. Details of the fabrication process for this device can be obtained from [15]. A silicon mirror plate (5 mm long $\times$ 5 mm wide $\times$ 0.4 mm thick) and a mechanical supporting silicon beam (3 mm long $\times$ 5 mm wide $\times$ 5 μm thick) integrated with 1×10 arrayed PZT cantilever actuators (3 mm long $\times$ 0.24 mm wide $\times$ 5 μm thick for each cantilever) arranged in parallel are formed after the release process. The ten cantilevers

Manuscript received May 01, 2010; revised June 08, 2010; accepted June 25, 2010. Date of publication July 15, 2010; date of current version August 20, 2010. This work was supported by the National University of Singapore under Grant R-263-000-475-112 and by GLOBALFOUNDRIES Singapore under a Ph.D. scholarship grant.

K. H. Koh and C. Lee are with the Department of Electrical and Computer Engineering, National University of Singapore, Singapore 119260 (e-mail: elelc@nus.edu.sg).

T. Kobayashi is with the National Institute of Advanced Industrial Science and Technology (AIST), Tsukuba, Ibaraki 305-8564, Japan.

Color versions of one or more of the figures in this letter are available online at http://ieeexplore.ieee.org.

Digital Object Identifier 10.1109/LPT.2010.2056679

1041-1135/$26.00 © 2010 IEEE

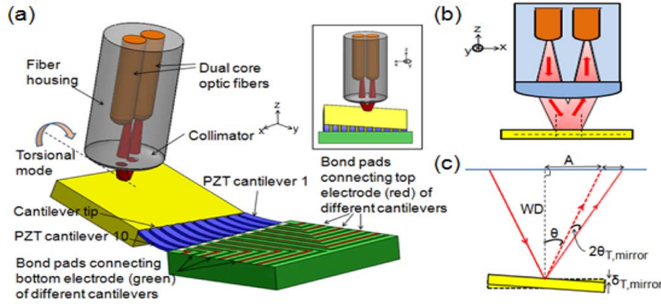

Fig. 1. Schematic drawing showing (a) PZT MEMS VOA with dual-core collimator arranged in 3-D configuration such that the light beam focuses on far edge center of mirror plate. Inset shows torsional mode where a set of five cantilevers bends in one direction while the other set of five cantilevers bends in the opposite direction. (b) configuration corresponding to initial state of minimum insertion loss. (c) mirror is rotated by an angle $\theta_{T,\mathrm{mirror}}$ and the laser beam is displaced by a distance $\delta_{T,\mathrm{laser}}$.

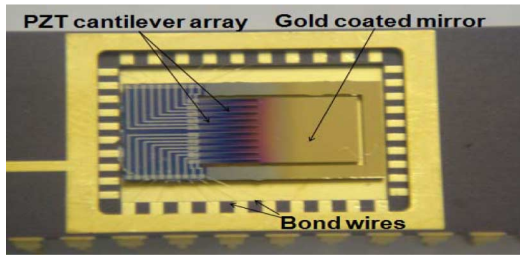

Fig. 2. Closed-up photo showing the packaged PZT MEMS VOA with a gold-coated mirror surface. The bond pads are connected to the pins of the package via gold bond wires.

are designed to be electrically isolated from one another, with individual bonding pads connected to each of the top and bottom electrodes of the cantilevers (Figs. 1(a) and 2).

The inset in Fig. 1(a) illustrates the device in torsional mode, where, for example, cantilevers 1–5 are biased in such a way that they bend down, while cantilevers 6–10 are biased to bend upward, i.e., the opposite direction. The difference in bending directions for the two sets of actuators causes the mirror to rotate along the x-z plane. Fig. 1(b) shows the front profile of the mirror and the dual-core fiber with collimator, where optimized light coupling occurs when the cantilevers are initially unbiased. The measured coupling loss during this initial state is referred to as insertion loss. Fig. 1(c) shows a simplified diagram of the reflected laser beam path in the torsional mode operation. The torsional rotation angle of the mirror $\theta_{T,\mathrm{mirror}}$, is related to the displacement of the laser beam from its original position by

$$\theta_{T,\mathrm{mirror}} = \tan^{-1}\left(\frac{2\delta_{T,\mathrm{mirror}}}{L_{\mathrm{mirror}}}\right) \tag{1}$$

$$\theta = \tan^{-1}\left(\frac{A}{\mathrm{WD}}\right) \tag{2}$$

$$\delta_{T,\mathrm{laser}} = \mathrm{WD} * \tan(\theta + 2\theta_T) - A \tag{3}$$

where $\delta_{T,\mathrm{mirror}}$ is the displacement of the mirror edges observed under an optical microscope, L_{mirror} is the length of the mirror plate (5 mm), A is the half distance between the input and output fiber (100 μm), and WD is the working distance of the dual core collimator (1 mm). These equations allow us to derive the displacement of the laser beam from its original position using the experimental $\delta_{T,\mathrm{mirror}}$ under torsional mode.

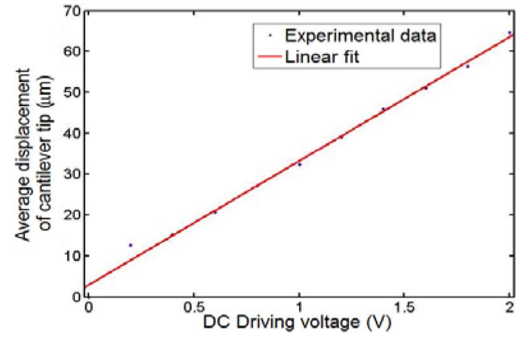

Fig. 3. Measured average displacement of cantilever tips versus dc driving voltage applied to the top electrodes of all ten cantilevers.

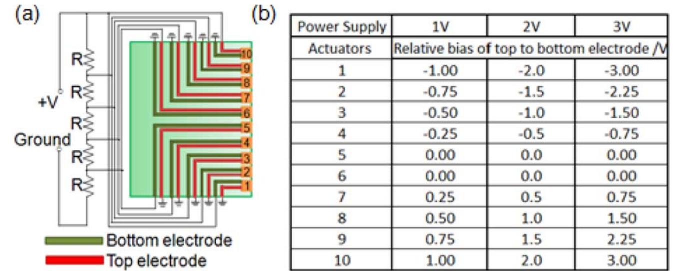

Power Supply	1V	2V	3V
Actuators	Relative bias of top to bottom electrode /V		
1	-1.00	-2.0	-3.00
2	-0.75	-1.5	-2.25
3	-0.50	-1.0	-1.50
4	-0.25	-0.5	-0.75
5	0.00	0.0	0.00
6	0.00	0.0	0.00
7	0.25	0.5	0.75
8	0.50	1.0	1.50
9	0.75	1.5	2.25
10	1.00	2.0	3.00

Fig. 4. (a) Schematic diagram illustrating the electrical connections of the top and bottom electrodes of each cantilever to the dc power supply. (b) Look-up table showing the individual dc bias driving each cantilever for a dc power supply voltage.

III. Experiments and Results

Fig. 2 shows the packaged MEMS mirror which is bonded onto a dual-in-line package (DIP) and the bond pads on the device were connected by gold bond wires to the metal pins of the DIP. To enhance the piezoelectric characteristics, poling treatment was conducted on the PZT thin film actuators at 30 V for 10 min at room temperature. In order to derive the value of transverse piezoelectric constant d_{31}, the ten cantilevers were biased simultaneously at the same dc driving voltage while the displacement of the ten cantilever tips were observed under the optical microscope. The measured displacements of ten cantilevers were averaged. This was repeated for various dc driving voltages and the results were plotted in Fig. 3. According to the linear fitting line and the approach discussed in [15], we derived d_{31} of the PZT thin films from a set of equations regarding to the average displacement changes when the voltage was decreased from 2 to 0 V. The transverse piezoelectric constant d_{31} is estimated as 113$\pm$3 pmV^{-1}.

Fig. 4(a) shows the biasing configuration to achieve torsional mode. A potential divider was implemented to split the dc power supply into five equal potential at the potential nodes between each resistors. The potential divider is realized using five equal resistors of resistance 20 Ω each connected in series. For the set of cantilevers 1–5, the top electrodes for these cantilevers are grounded while the bottom electrodes are connected to different potential nodes. For the set of cantilevers 6–10, the top electrodes are connected to the various potential nodes while the

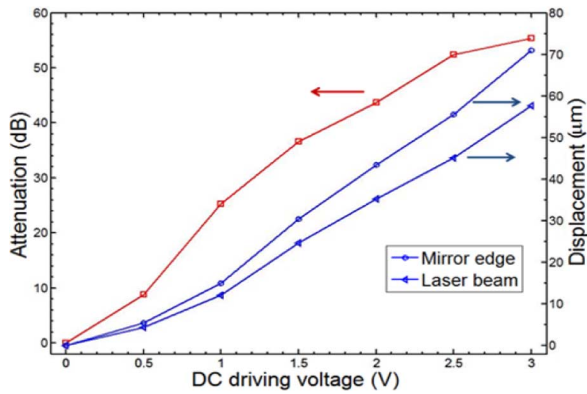

Fig. 5. Red curve shows measured attenuation curves versus dc driving voltage of power supply. Blue curves show the displacements of mirror edge and laser beam versus dc driving voltage of power supply.

bottom electrodes are grounded. As such, each of the cantilevers in both bias cases A and B will have a different dc bias value as evident from the look-up table in Fig. 4(b). This results in largest and zero cantilever displacement introduced at the mirror edges and center, respectively. More importantly, the generated displacements for the two sets of cantilevers are towards the opposite direction, resulting in torsional rotation of the mirror. Prior to deriving the attenuation characteristic, the packaged device is first mounted on an x-y-z-θy-θz stage and the relative position of the mirror to the collimator is adjusted by moving and tilting the stage such that minimum insertion loss is reached. The θy and θz adjustment knobs enable the tilting of the stage with respect to the y- and z-axis, respectively. A 1550-nm light source is used in this experiment. The measured initial insertion loss in this setup is typically about 2–3 dB, which is mainly attributed to the surface roughness and warpage of the mirror. Further optimization of the mirror fabrication and microstructures may reduce the initial insertion loss to be less than 1 dB.

The red curve in Fig. 5 shows the measured attenuation curve versus dc voltage of the power supply. A dynamic attenuation range of 40 dB was achieved at a bias of 1.8 V. In addition, the attenuation curve follows weakly that of a Gaussian distribution. This is due to the use of a Gaussian laser beam, where the intensity of the beam is normal distributed from the center of the beam. The absolute value for the displacements of the two opposite edges of the mirror $\delta_{T,\mathrm{mirror}}$ were measured, averaged, and repeated for different dc driving voltage of power supply. The results are shown as the blue middle curve. The bottom-right blue curve shows laser beam displacement $\delta_{T,\mathrm{Laser}}$ derived by substituting the obtained mirror edge displacement $\delta_{T,\mathrm{mirror}}$ into (1)–(3). It is observed that the mirror edge displacement and laser beam displacement of 32 and 38 μm were derived at a dc driving voltage of 1.8 V, respectively, in order to achieve 40-dB attenuation.

Improvements to the attenuation performance can be made by adopting the PZT cantilever structure fabricated in [16], where Isakaron *et al.* obtained a d_{31} value of 130 pmV^{-1} based on 0.1-μm-thick PZT thin film. This will possibly reduce the dc driving voltage for 40-dB attenuation from 1.8 to 1.56 V.

IV. Conclusion

In this study, a novel piezoelectric driven 3-D VOA using mechanical supporting beam integrated with multiple cantilever actuators was explored and characterized in a 3-D attenuation configuration. Torsional mirror rotation based on the relative difference in displacements under dc bias for the ten piezoelectric cantilever actuators is demonstrated. The transverse piezoelectric constant d_{31} has been estimated to be 113 pmV^{-1}. A dynamic attenuation range of 40 dB was achieved at 1.8 V, with an approximate mirror edge and laser beam displacement of 32 and 38 μm obtained, respectively.

References

[1] A. Q. Liu and X. M. Zhang, “A review of MEMS external-cavity tunable lasers,” *J. Micromech. Microeng.*, vol. 17, pp. R1–R13, 2007.

[2] Y.-J. Yang, B.-T. Liao, and W.-C. Kuo, “A novel 2 × 2 MEMS optical switch using the split cross-bar design,” *J. Micromech. Microeng.*, vol. 17, pp. 875–882, 2007.

[3] C. Antoine, X. Li, J.-S. Wang, and O. Solgaard, “Reconfigurable optical wavelength multiplexer using a MEMS tunable blazed grating,” *J. Lightw. Technol.*, vol. 25, pp. 3001–3007, Oct. 2007.

[4] J. A. Walker, K. W. Gossen, and S. C. Arney, “Fabrication of a mechanical antireflection switch for fiber-to-home systems,” *J. Microelectromech. Syst.*, vol. 5, pp. 45–51, 1996.

[5] B. Barber, C. R. Giles, V. Askyuk, R. Ruel, L. Stulz, and D. Bishop, “A fiber connectorized MEMS variable optical attenuator,” *IEEE Photon. Technol. Lett.*, vol. 10, no. 9, pp. 1262–1264, Sep. 1998.

[6] C. Marxer, P. Griss, and N. F. de Rooij, “A variable optical attenuator based on silicon micromechanics,” *IEEE Photon. Technol. Lett.*, vol. 11, no. 2, pp. 233–235, Feb. 1999.

[7] S. H. Hung, H.-T. Hsieh, and G.-D. J. Su, “An electro-magnetic micromachined actuator monolithically integrated with a vertical shutter for variable optical attenuation,” *J. Micromech. Microeng.*, vol. 18, p. 075003, Jul. 2008.

[8] H. Cai, X. M. Zhang, C. Lu, A. Q. Liu, and E. H. Khoo, “Linear MEMS variable optical attenuator using reflective elliptical mirror,” *IEEE Photon. Technol. Lett.*, vol. 17, no. 2, pp. 402–404, Feb. 2005.

[9] C. Lee, “A MEMS VOA using electrothermal actuators,” *J. Lightw. Technol.*, vol. 25, no. 2, pp. 490–498, Feb. 2007.

[10] K. Isamoto, K. Katom, A. Morosawa, C. Chong, H. Fujita, and H. Toshiyoshi, “A 5-V operated MEMS variable optical attenuator by SOI bulk micromaching,” *IEEE J. Sel. Topics Quantum Electron.*, vol. 10, no. 3, pp. 570–578, May/Jun. 2004.

[11] W. Sun, W. Noell, M. Zickar, M. J. Mughal, F. Perez, N. A. Riza, and N. F. de Rooij, “Design, simulation, fabrication and characterization of a digital variable optical attenuator,” *J. Microelecromech. Syst.*, vol. 15, pp. 1190–1200, 2006.

[12] C. Lee, F.-L. Hsiao, T. Kobayashi, K. H. Koh, P. V. Ramana, W. Xiang, B. Yang, C. W. Tan, and D. Pinjala, “A 1-V operated MEMS variable optical attenuator using piezoelectric PZT thin-film actuators,” *IEEE J. Sel. Topics Quantum Electron.*, vol. 15, no. 5, pp. 1529–1536, Sep./Oct. 2009.

[13] A. Jain, H. Qu, S. Todd, and H. Xie, “A thermal bimorph micromirror with large bidirectional and vertical actuation,” *Sens. Actuators A, Phys.*, vol. 122, no. 1, pp. 9–15, Jul. 2005.

[14] D. H. Kim, Y. C. Park, and S. Park, “Design and fabrication of twisting-type thermal actuation mechanism for micromirrors,” *Sens. Actuators A*, vol. 159, no. 1, pp. 79–87, 2010.

[15] T. Kobayashi, M. Ichiki, T. Noguchi, K. Nakamura, and R. Maeda, “Fabrication of piezoelectric microcantilevers using $LaNiO_3$ buffered $Pb(Zr,Ti)O_3$ thin film,” *J. Micromech. Microeng.*, vol. 18, pp. 035007-1–035007-5, 2008.

[16] D. Isarakorn, A. Sambri, P. Janphuang, D. Briand, S. Gariglio, J.-M. Triscone, F. Guy, J. W. Reiner, C. H. Ahn, and N. F. de Rooij, “Epitaxial piezoelectric MEMS on silicon,” *J. Micromech. Microeng.*, vol. 20, p. 055008, 2010, (9 pp.).